PAAT

PROGRESS IN AEROSPACE AND AVIATION TECHNOLOGY
e-ISSN: 2821-2924

Vol. 6 No. 1 (2026) 47-59
https://publisher.uthm.edu.my/ojs/index.php/paat

One-Way Fluid-Structure Interaction Study of a Movable Rocket Fin at Various Cant Angles for Aerodynamic Performance and Stability Analysis Under Transient Conditions

Yau Sheng Lim[1], Mohd Fadhli Zulkafli[2]*

[1] *Faculty of Mechanical and Manufacturing Engineering, Universiti Tun Hussein Onn Malaysia, 86400 Parit Raja, Johor, MALAYSIA*
[2] *Research Center for Unmanned Vehicles (RECUV), Faculty of Mechanical and Manufacturing Engineering, Universiti Tun Hussein Onn Malaysia (UTHM), Batu Pahat, 86400, MALAYSIA*

*Corresponding Author: fadhli@uthm.edu.my
DOI: https://doi.org/10.30880/paat.2026.06.01.006

Article Info

Received: 1 January 2026
Accepted: 12 May 2026
Available online: 30 June 2026

Keywords

Rocket fin, cant angle, fluid-structure interaction, transient conditions, aerodynamic performance, stability, ANSYS Fluent

Abstract

This study investigates the aerodynamic performance and flow behavior of a movable rocket fin at various cant angles under transient conditions using a one-way fluid-structure interaction (FSI) simulation approach. The rocket fin and simplified cylindrical rocket body were modeled in SolidWorks 2025 and imported into ANSYS DesignModeler to create the surrounding fluid domains and computational mesh. Two domains were used: a stationary rectangular outer domain and a rotating cylindrical inner domain around the fin to enable sliding-mesh motion. The meshed domains were then imported into ANSYS Fluent for transient CFD simulation. The cylindrical domain was assigned a constant angular velocity so that the fin rotated from 0° to 15° during the simulation. The results show that increasing the fin cant angle changes the pressure distribution, velocity field, turbulence kinetic energy, aerodynamic forces, aerodynamic moments, and wake structures around the fin. The findings indicate that transient simulation of a prescribed movable fin can aid in understanding how cant-angle variation influences rocket-fin aerodynamic performance and stability.

1. Introduction

Rocket fins are critical components for maintaining rocket stability and providing passive aerodynamic guidance along the intended flight trajectory. A properly designed fin generates restoring aerodynamic forces and moments that counter unwanted rotation and help maintain directional stability [6], [8], and [9]. Consequently, fin geometry, including cant angle, strongly influences rocket aerodynamic performance and stability during flight.

Previous studies have examined rocket-fin geometry, fin shape, nose-cone configuration, and cant-angle effects using analytical methods, computational fluid dynamics (CFD), and flight-stability analysis [1], [4], [5], [8], [11], [12], [13], [15]. These studies show that fin configuration affects drag, lift, stability margin, and trajectory behavior; however, many of them considered fixed fin orientations or steady-flow conditions. Cant-angle variation can alter the pressure distribution, induce asymmetric flow structures, and change the aerodynamic forces and moments acting on the vehicle [3], [10], [12]-[14]. Therefore, a transient numerical approach is required to capture the flow response when a movable fin rotates from its initial position to a prescribed cant angle.

This study develops a three-dimensional, one-way fluid-structure interaction (FSI) model of a rocket body and movable rocket fin to simulate the influence of fin rotation on aerodynamic force, moment, pressure distribution, velocity field, turbulence kinetic energy, and flow behavior under transient conditions. FSI and unsteady-aerodynamic studies are useful for representing time-dependent fluid loading and its interaction with rocket or aerospace structures [2], [7], [16], [17]. In the present work, the rocket fin is treated as a rigid body; therefore, the moving fin affects the surrounding fluid, but structural deformation caused by aerodynamic loading is not modeled. In contrast with previous CFD studies in which each cant angle was analyzed separately as a fixed geometry [12], [13], the present simulation rotates the fin dynamically from 0° to 15° so that the transient aerodynamic response can be observed directly.

2. Methodology

2.1 Rocket and Fin Geometry

The rocket body and fin geometry were adopted from previous low-altitude rocket studies that investigated fin cant angle and fin-height effects on rocket stability and performance [12], [13]. As shown in Fig. 1(a), the rocket body was simplified as a cylinder with a length of 45 in and a diameter of 3 in rather than modeled using the full rocket geometry. This simplification reduced the computational cost and allowed the analysis to focus on the aerodynamic effect of the movable fin. The fin geometry in Fig. 1(b) has a 3-inch tip chord, a 3-inch span, a 6-inch root chord attached to the rocket body, a 45° sweep angle, and a thickness of 0.2 inches. Before the fluid domains were generated, the geometry was cleaned to remove gaps between surfaces because such gaps may prevent successful Boolean subtraction and mesh generation in ANSYS.

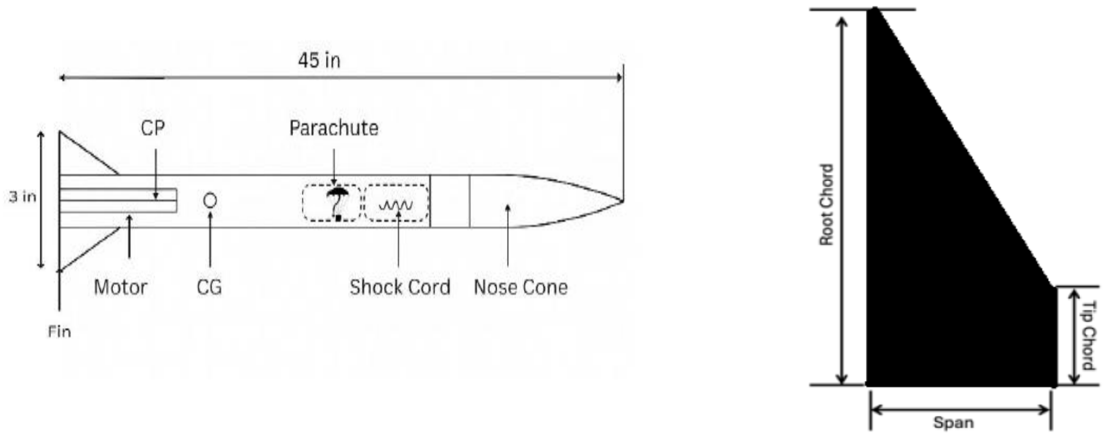

(a) **(b)**

Fig. 1 *(a) Rocket model; (b) Rocket fin design*

2.2 Fluid Domain and Mesh Generation

After the rocket body and fin geometries were imported into ANSYS DesignModeler, two fluid domains were created, as illustrated in Fig. 2. The first domain was a stationary rectangular outer domain with a width and height of 20 in and a length of 200 in. The second domain was a rotating cylindrical inner domain with a radius of 4 in and a height of 4 in. The rectangular domain enclosed the rocket body, the fin, and the cylindrical rotating domain, whereas the cylindrical domain enclosed the fin and the surrounding portion of the rocket body. Boolean subtraction was applied to both domains. The cylindrical domain and rocket body were used as cutters for the rectangular domain to create the external flow passage, while the fin and the portion of the rocket body inside the cylindrical domain were used as cutters for the rotating domain.

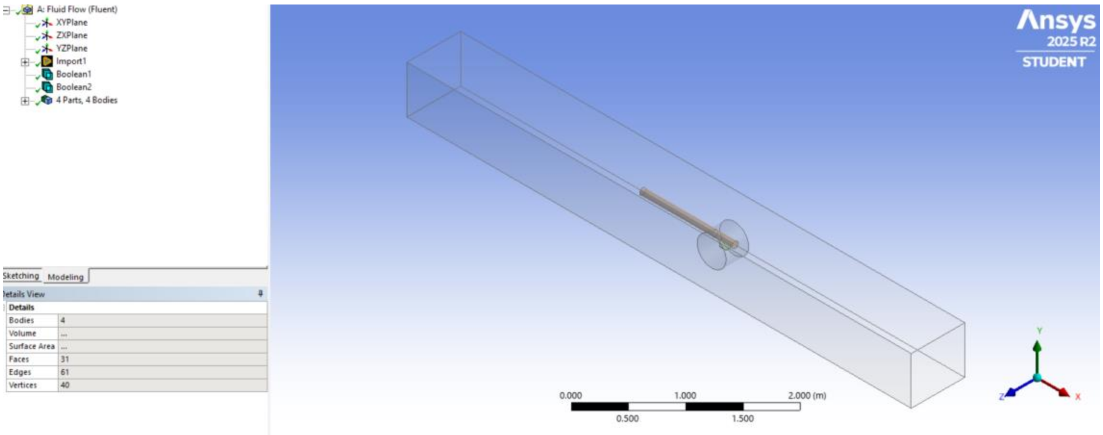

Fig. 2 *Fluid domain*

The inlet and outlet were assigned at the two ends of the rectangular domain to define the airflow path. Before meshing, the solid rocket body and fin were suppressed, and the fin wall and body wall were named as boundary surfaces that interact with the fluid. The interfaces between the stationary and rotating zones were also named to ensure proper connection during the sliding-mesh simulation. Figs. 3(a) and 3(b) show the generated meshes for the rectangular and cylindrical domains, respectively. An automatic meshing method was selected for both domains because the geometry contains sharp edges and local curvature. The target skewness was set to 0.8, and orthogonal quality was used as the mesh metric to reduce the likelihood of poor-quality cells and negative cell-volume errors. The global mesh size for the rectangular domain was set to 1 in, while a finer body size of 0.6 in was assigned to the cylindrical domain. The stationary-zone and rotating-zone interface surfaces were meshed using element sizes of 0.8 in and 0.6 in, respectively. Proximity and curvature capture were enabled for the cylindrical domain to improve mesh resolution near the fin and rotating interface.

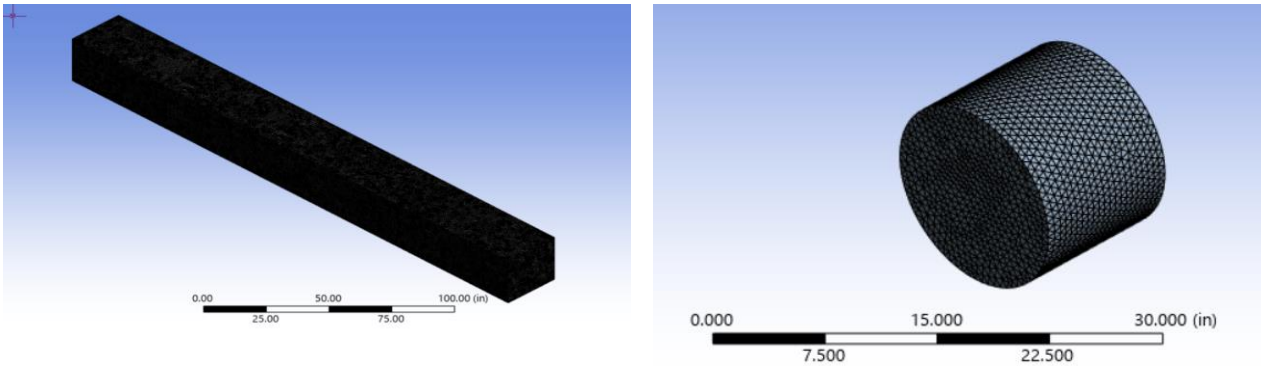

(a) **(b)**

Fig. 3 *(a) Meshing of rectangular fluid domain; (b) Meshing of cylindrical fluid domain*

2.3 Simulation Setup, Solution Procedure, and Post-Processing

ANSYS Fluent was used to set up, solve, and post-process the transient simulation of the movable rocket fin. The solver was configured as pressure-based, transient, and absolute velocity-based. Air was modeled as a single-phase fluid, and the shear-stress transport (SST) k-omega turbulence model was selected for the simulation. Mesh motion was activated only for the cylindrical domain to enable sliding-mesh rotation of the fin from 0° to 15° at a constant angular velocity of 0.01745 rad/s. The rotation axis was defined using the x-, y-, and z-axis coordinates of -3, 0, and 3, respectively, with the z-axis rotation direction set to 1. The inlet airflow velocity was 147.52 m/s under standard atmospheric conditions. The fin and body walls were assigned no-slip stationary-wall boundary conditions, while the rectangular domain, fin wall, and body wall were maintained as stationary zones in the dynamic-mesh setup.

The numerical solution used SIMPLE pressure-velocity coupling with Rhie-Chow momentum-based flux interpolation. The spatial discretization schemes were least-squares cell-based gradients, second-order pressure, second-order MUSCL momentum, second-order MUSCL turbulent kinetic energy, and second-order MUSCL specific dissipation rate. A first-order implicit scheme was used for the transient formulation. Warped-face gradient correction and high-order term relaxation were enabled to improve solution stability. Report definitions were created to calculate drag, lift, moment, and their corresponding coefficients. Simulation data was saved every five time steps. The total number of time steps was 150; the time-step size was 0.01 s; and the maximum number of iterations per time step was 20. The calculation was started after all boundary conditions were defined and hybrid initialization was completed.

3. Results and Discussion

3.1 Grid Independence Study

Three mesh resolutions were evaluated in the grid-independence study. The number of elements was increased by reducing the mesh size, and the drag, lift, and moment at the final time step, corresponding to a cant angle of 15°, were compared. Table 1 summarizes the number of elements and the corresponding aerodynamic quantities for the three grid tests. The drag, lift, and moment gradually converged as the number of elements increased. As shown in Fig. 4, the aerodynamic moment changed only slightly when the number of cells increased to 765,354. Therefore, the third mesh was selected for the transient simulation because it provided more consistent results while maintaining a reasonable computational cost.

Table 1 *Grid-independence results for drag, lift, and moment*

Number of Elements	Drag (N)	Lift (N)	Moment (Nm)
301574	19.9638	-70.4114	6.0272
605069	21.6115	-76.3700	6.5141
765354	21.7181	-76.4333	6.5382

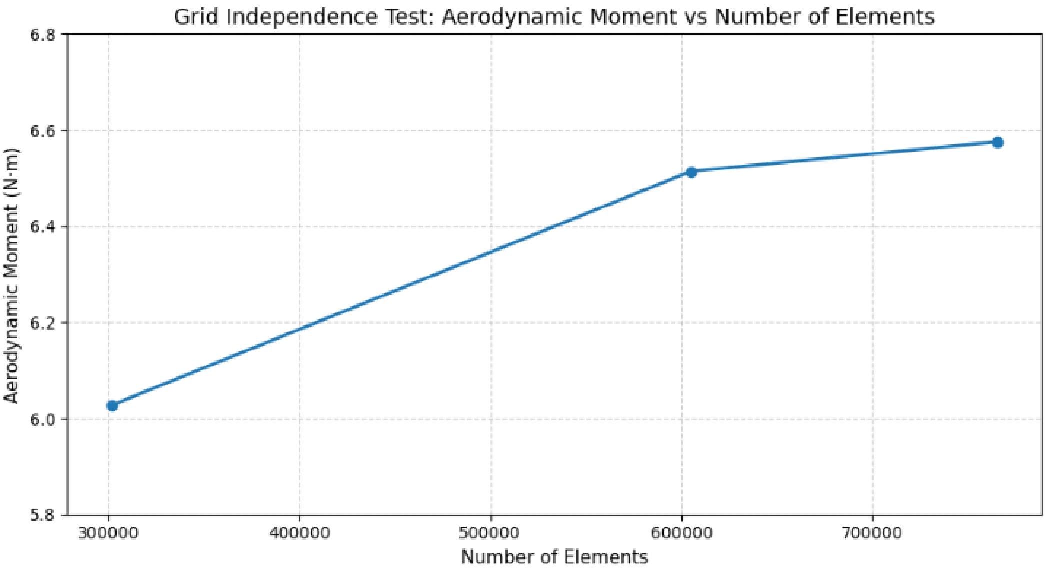

(a)

Fig. 4 *Grid independence test of moment vs. number of elements*

3.2 Pressure Distribution and Flow Behavior

Fig. 5 presents the pressure contours on the XY plane for cant angles from 0° to 15°. The red regions indicate higher pressure, whereas the blue regions indicate lower pressure. At the initial 0° position, the pressure field is approximately symmetric about the fin. As the cant angle increases, the pressure field becomes increasingly nonuniform and asymmetric. The high-pressure region expands above the fin, while the low-pressure region develops below the fin. This trend indicates that the pressure difference across the fin increases with cant angle, which contributes to higher aerodynamic loading and a larger moment.

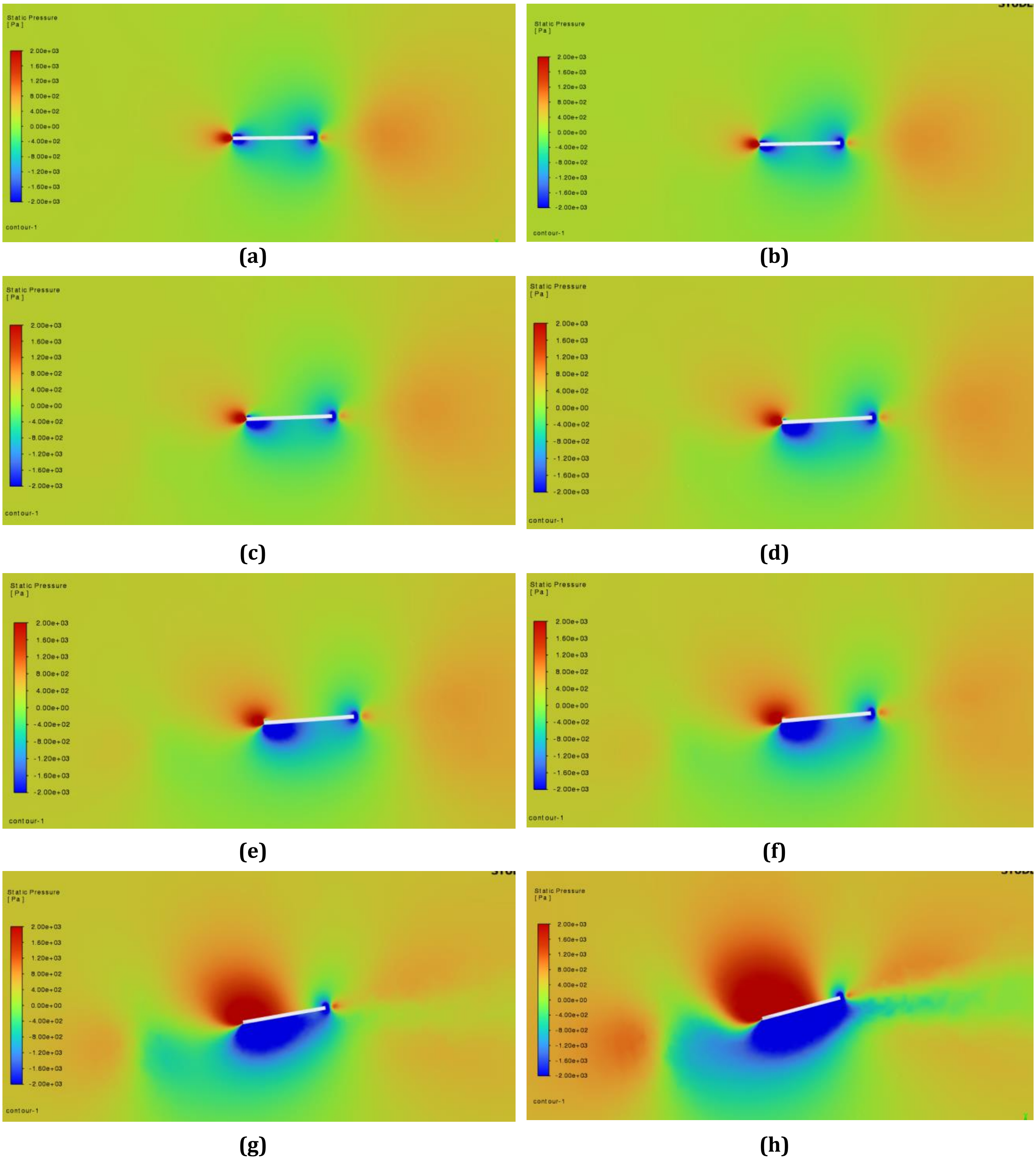

Fig. 5 *Pressure contour at XY plane (a) 0°; (b) 1°; (c) 2°; (d) 3°; (e) 4°; (f) 5°; (g) 10°; (h) 15°*

3.3 Velocity Contours and Flow Behavior

The velocity contours on the YZ and XY planes were examined to evaluate how the changing cant angle affects the airflow around the fin. In the contour plots, red denotes higher velocity and blue denotes lower velocity. Three YZ-plane locations were considered: near the leading edge, at the mid-span region of the fin, and near the trailing edge. These locations are compared in Figs. 6-8, respectively.

The YZ-plane velocity contours in Figs. 6-8 show a similar overall trend. At 0°, the flow is relatively uniform, and only a small disturbance appears near the fin. As the cant angle increases, the low-velocity region expands downward, and the wake becomes increasingly asymmetric. At 15°, a stronger disturbance and a larger separated-wake region are formed behind the fin, indicating more pronounced flow separation under transient fin rotation.

The magnitude of velocity reduction and wake development also depends on the fin location. Near the leading edge, shown in Fig. 6, flow separation is weaker because the airflow has just begun to interact with the fin. At the middle location, shown in Fig. 7, the wake and separated region are larger than those near the leading edge. The strongest wake development occurs near the trailing edge, shown in Fig. 8, because this region encounters the cumulative downstream effect of the disturbed flow. These observations indicate that the trailing-edge region is the most sensitive to cant-angle-induced flow separation.

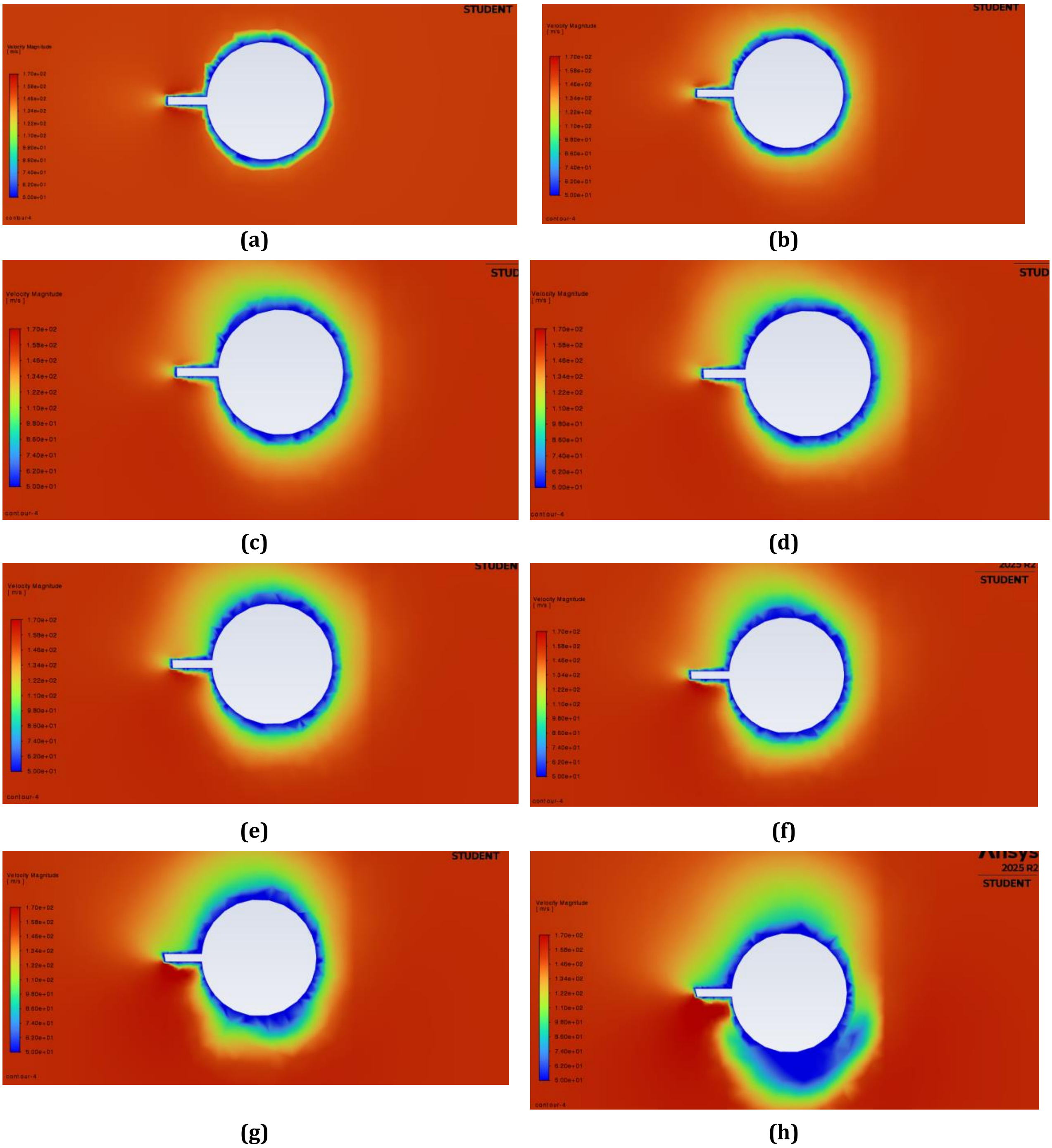

Fig. 6 *Velocity contour at YZ plane near leading edge (a) 0°; (b) 1°; (c) 2°; (d) 3°; (e) 4°; (f) 5°; (g) 10°; (h) 15°*

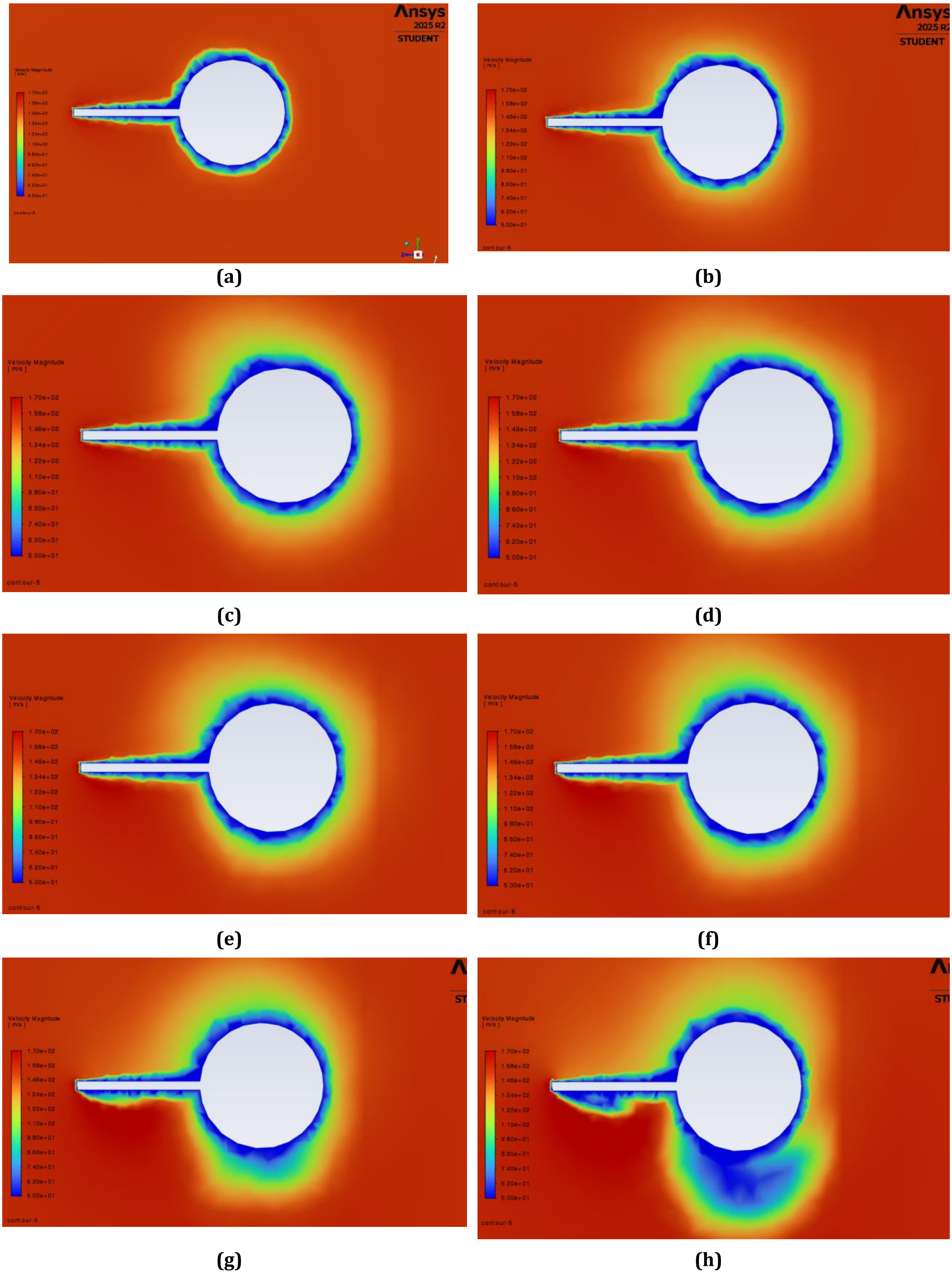

Fig. 7 *Velocity contour at YZ plane at middle fin: (a) 0°; (b) 1°; (c) 2°; (d) 3°; (e) 4°; (f) 5°; (g) 10°; (h) 15°*

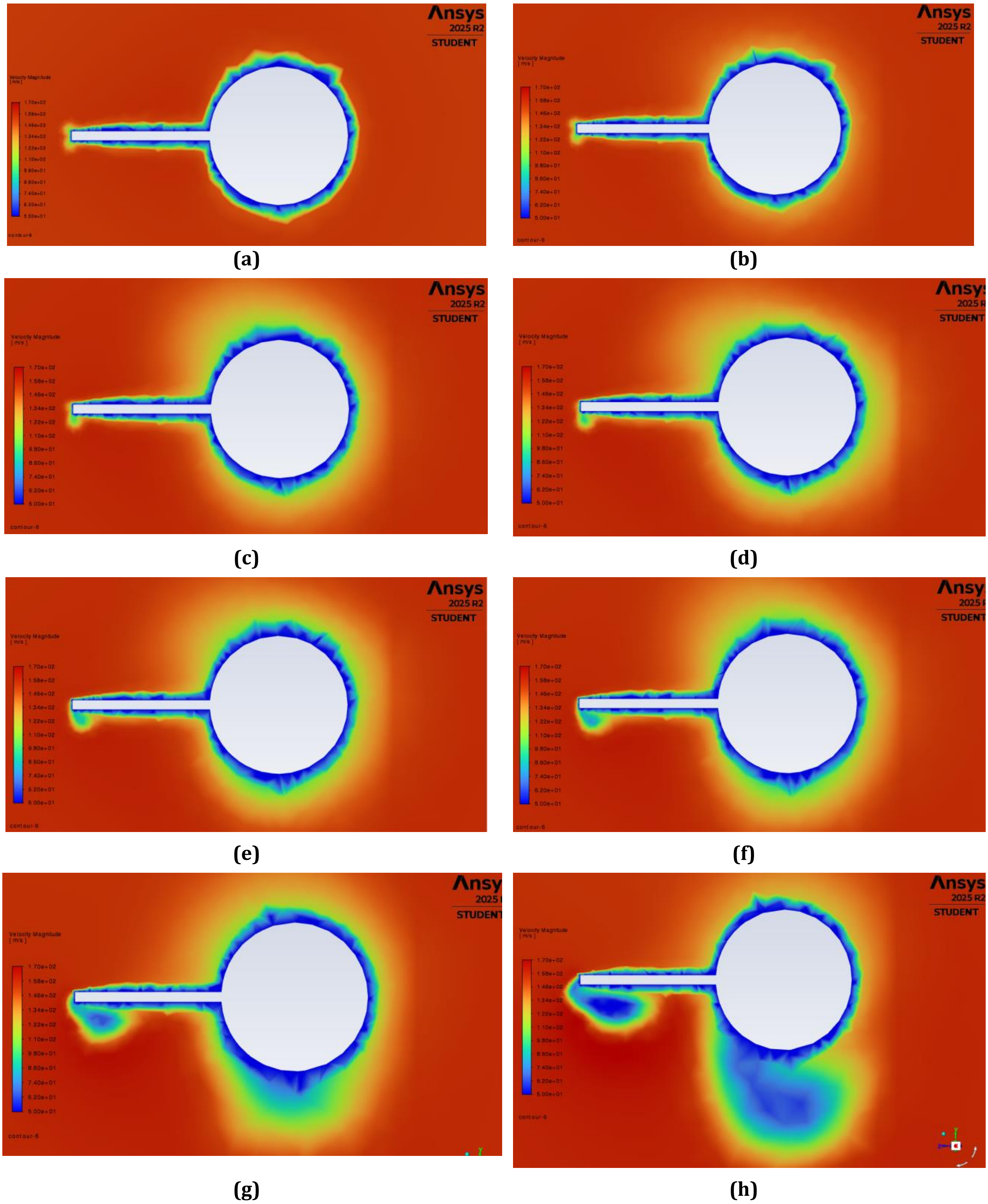

Fig. 8 *Velocity contour at YZ plane near trailing edge (a) 0°; (b) 1°; (c) 2°; (d) 3°; (e) 4°; (f) 5°; (g) 10°; (h) 15°*

The XY-plane velocity contours in Fig. 9 provide an additional view of the wake generated behind the fin. Similar to the YZ-plane results, the airflow is nearly symmetric when the fin is at 0°. As the cant angle increases, the low-velocity region expands downward, and the wake becomes more asymmetric. The XY-plane view more clearly illustrates the downstream wake growth behind the fin as the cant angle increases.

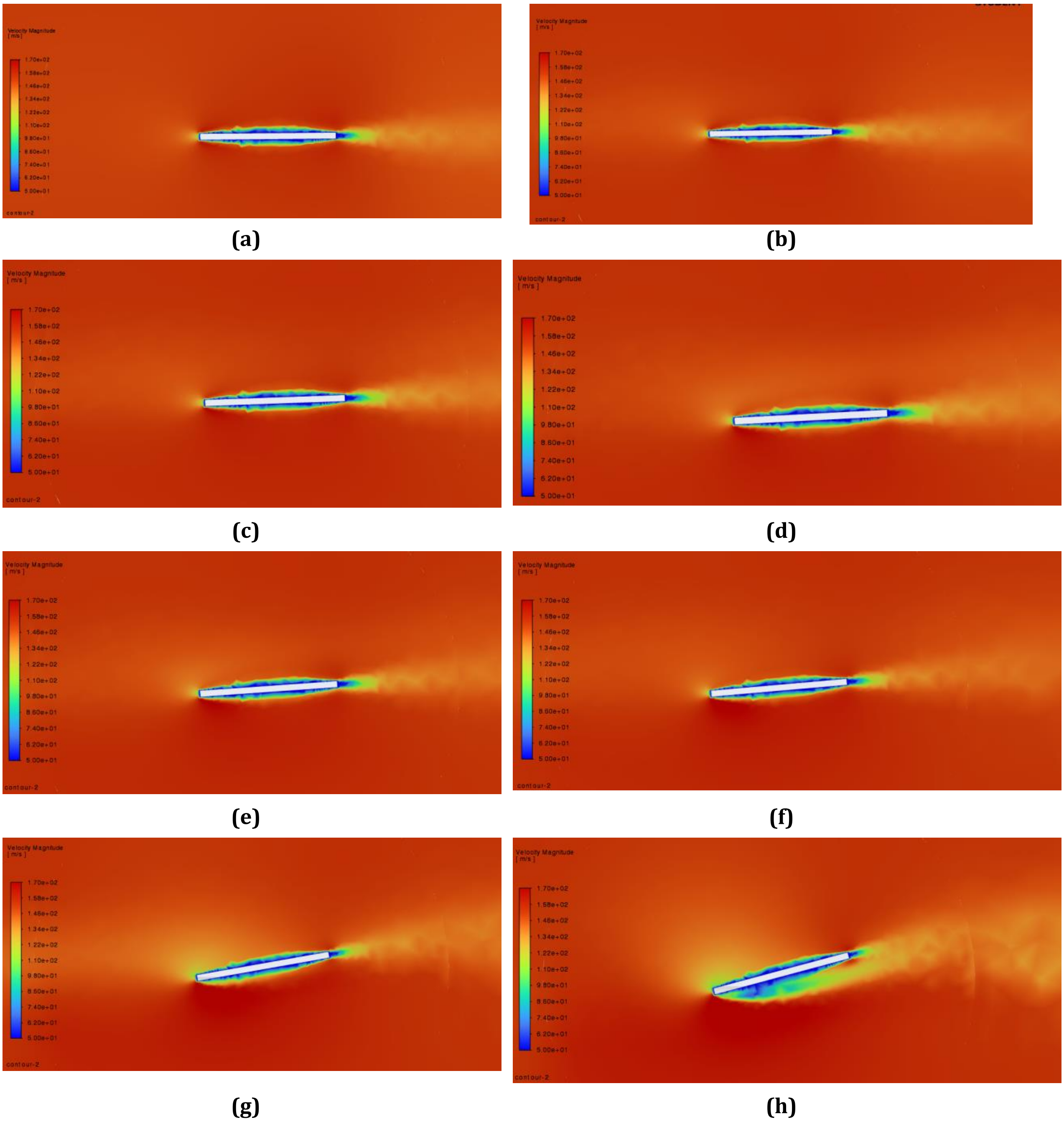

Fig. 9 *Velocity contour at XY plane: (a) 0°; (b) 1°; (c) 2°; (d) 3°; (e) 4°; (f) 5°; (g) 10°; (h) 15°*

3.4 Turbulence Kinetic Energy Contours

Fig. 10 shows the turbulence kinetic energy contours on the XY plane. The red regions indicate higher turbulence kinetic energy, whereas the blue regions indicate lower turbulence kinetic energy. The results show that turbulence kinetic energy increases as the fin rotates from 0° to 15°. The yellow, green, and red regions progressively expand around and downstream of the fin, replacing the initially low-intensity blue region. At 15°, a long high-turbulence wake forms downstream of the fin, indicating that the largest cant angle produces the strongest flow disturbance and wake development.

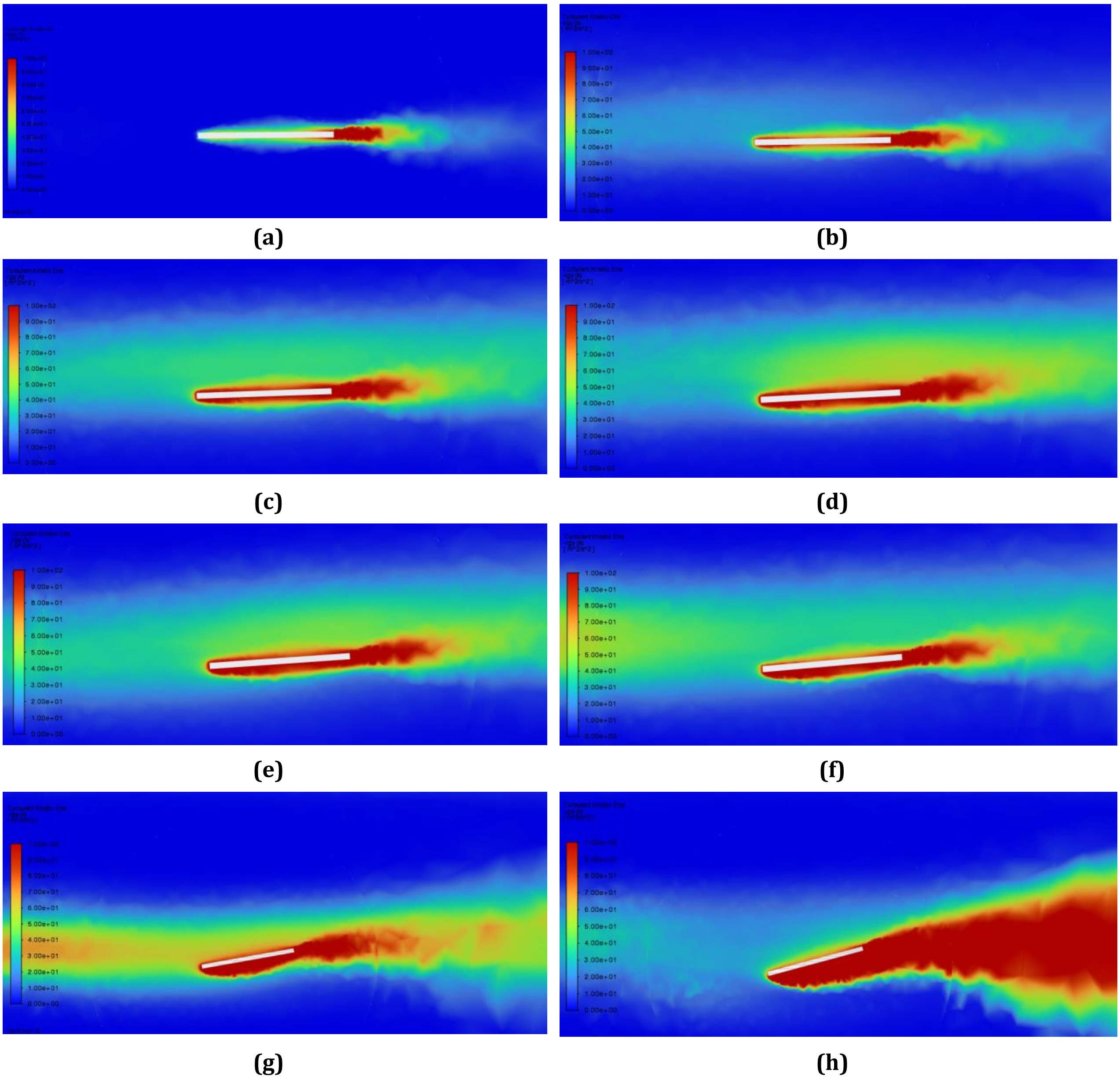

Fig. 10 *Turbulence kinetic energy contour at XY Plane (a) 0°; (b) 1°; (c) 2°; (d) 3°; (e) 4°; (f) 5°; (g) 10°; (h) 15°*

3.5 Effect of Cant Angle on Aerodynamic Forces and Moments

Figs. 11-13 show the lift coefficient and lift, drag coefficient and drag, and moment coefficient and moment, respectively. The results indicate that increasing the cant angle increases the magnitudes of all aerodynamic coefficients and forces. The negative sign of the lift coefficient and lift represents the negative lift direction defined in ANSYS Fluent. The aerodynamic moment increases as the cant angle increases because the combined effects of lift and drag generate a stronger rotational tendency. Although a larger cant angle can increase aerodynamic effectiveness, it also increases drag and produces stronger wake development. Therefore, cant-angle selection should balance stability and control effectiveness against the drag penalty and wake growth.

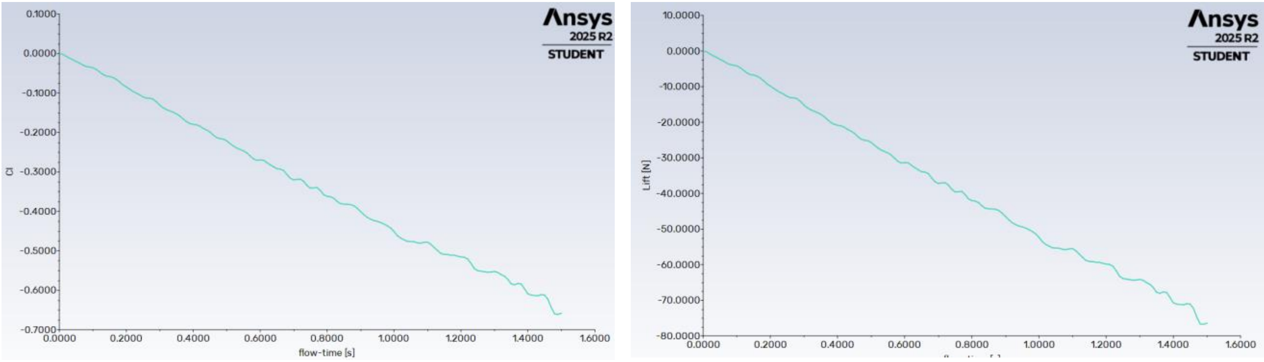

(a) **(b)**

Fig. 11 *(a) Lift coefficient; (b) Lift*

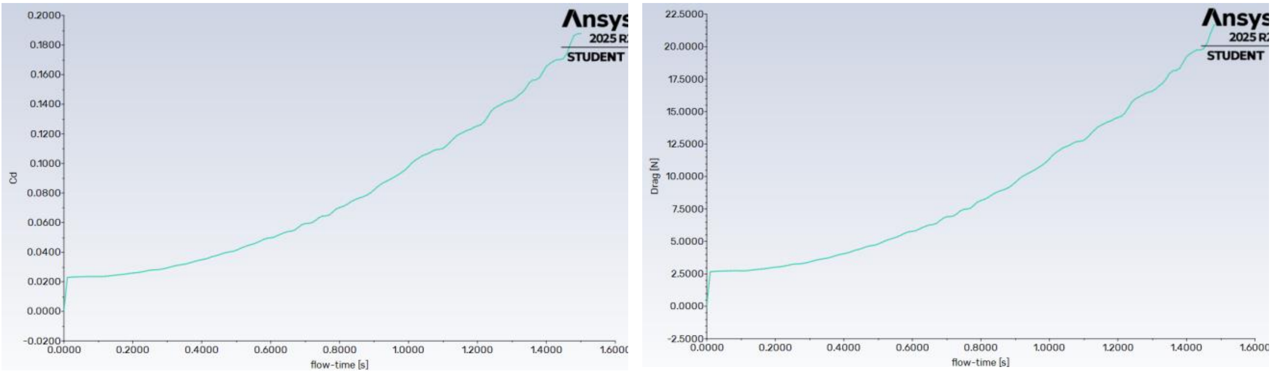

(a) **(b)**

Fig. 12 *(a) Drag coefficient; (b) Drag*

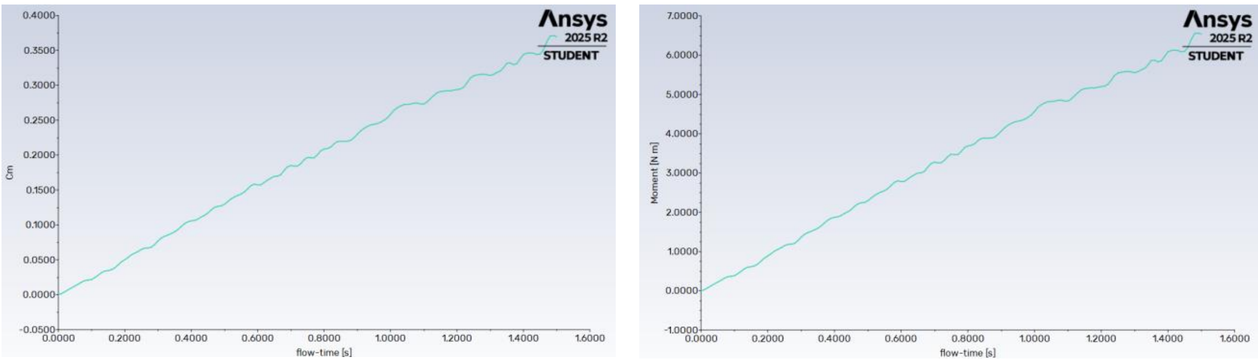

(a) **(b)**

Fig. 13 *(a) Moment coefficient; (b) Moment*

4. Conclusion

This study successfully developed a three-dimensional, one-way FSI model of a movable rocket fin and simulated its transient rotation from 0° to 15°. The model captured the aerodynamic response of the rocket fin without numerical errors such as floating-point errors or negative cell volumes. The simulation framework therefore provides a suitable basis for evaluating how fin cant-angle variation affects aerodynamic performance and flow behavior under transient conditions.

The results show that cant angle variation significantly affects aerodynamic force, aerodynamic moment, pressure distribution, velocity field, turbulence kinetic energy, and wake development. Increasing the cant angle increases the magnitudes of lift and moment, which may improve aerodynamic control effectiveness. However, the same increase also raises drag and strengthens flow separation, which can reduce aerodynamic efficiency.

Overall, the pressure, velocity, and turbulence kinetic energy contours demonstrate that a larger cant angle produces stronger asymmetric flow and a more extensive wake around the fin. Therefore, the most suitable cant angle should be selected according to the intended rocket configuration, stability requirement, and performance specification. The developed transient simulation model can support future rocket-fin design studies by providing clearer insight into the relationship between movable fin rotation, aerodynamic loading, and stability.

Acknowledgment

The authors gratefully acknowledge the Faculty of Mechanical and Manufacturing Engineering, Universiti Tun Hussein Onn Malaysia, for providing the resources and support needed to complete this study.

Conflict of Interest

The authors declare that there is no conflict of interest regarding the publication of this paper.

Author Contribution

The authors confirm the following contributions to the paper: ***study conception and design:*** *Yau Sheng Lim and Mohd Fadhli Zulkafli;* ***data collection:*** *Mohd Fadhli Zulkafli;* ***analysis and interpretation of results:*** *Yau Sheng Lim and Mohd Fadhli Zulkafli; and* ***draft manuscript preparation:*** *Yau Sheng Lim and Mohd Fadhli Zulkafli. All authors reviewed the results and approved the final version of the manuscript.*

References

[1] A. A. Adnan, A. H. Abdul Hamid, Z. Salleh, and M. Z. Azizi, "Mathematical and computational fluid dynamics analysis of low-altitude rocket drag for various fin configurations," Journal of Aeronautics, Astronautics and Aviation, vol. 56, no. 3, pp. 781-790, 2024, doi: 10.6125/JoAAA.202407_56(3).12.

[2] M. I. Afridi et al., "Fluid-structure interaction in engineering based on its applications: A plenary and up-to-date review," Physics of Fluids, vol. 36, no. 10, pp. 1-35, 2024, doi: 10.1063/5.0234435.

[3] A. Abdullah, M. F. Zulkafli, M. A. Abdul Halim, R. A. Thanneermalai, and B. Basuno, "Aerodynamic optimization and thermal deformation effects on mid-altitude sounding rockets: A computational and structural analysis," Dynamics, vol. 5, no. 3, Art. no. 28, 2025, doi: 10.3390/dynamics5030028.

[4] A. D. N. Barokah et al., "A comparative analysis of aerodynamic performance: Straight fin and curved fin rockets using computational fluid dynamics (CFD)," Journal of Advanced Research in Fluid Mechanics and Thermal Sciences, vol. 115, no. 1, pp. 1-18, 2024, doi: 10.37934/arfmts.115.1.118.

[5] A. Datye, "Fin optimization for enhanced flight performance of an experimental rocket," in Proc. National Conference on Undergraduate Research (NCUR), University of Central Oklahoma, 2018, pp. 5-10.

[6] V. I. Feodosiev and G. B. Siniarev, "The basic principles of stabilization and steering," in Introduction to Rocket Technology, 1959, pp. 273-321, doi: 10.1016/B978-1-4832-3201-0.50014-0.

[7] U. Gulcat, Fundamentals of Modern Unsteady Aerodynamics. Berlin, Germany: Springer, 2011, doi: 10.1007/978-3-642-14761-6.

[8] A. Hussein Abdul Hamid et al., "The effect of different designs of fins and nose cones toward the stability and performance of a sugar rocket," International Transaction Journal of Engineering, vol. 13, no. 13, pp. 1-15, 2022, doi: 10.14456/ITJEMAST.2022.262.

[9] V. Lorenzo, "Static and dynamic analysis of the aerodynamic stability and trajectory simulation of a student sounding rocket," M.S. thesis, Universitat Politecnica de Catalunya, 2014.

[10] M. A. McDaniel, C. Evans, and D. J. Lesieutre, "The effect of tail fin parameters on the induced roll of a canard-controlled missile," in Proc. 28th AIAA Applied Aerodynamics Conf., 2010, pp. 1-17, doi: 10.2514/6.2010-4226.

[11] A. Pektas, Z. Demircan, U. Haciabdullahoglu, N. Ejder, and C. Tola, "Effects of different fin shapes on apogee and stability of model rockets," 2019.

[12] Z. Salleh, U. A. F. M. Asy'ari, A. H. A. Hamdi, M. A. Muhammad, and Z. A. Ghaffar, "Low-altitude rocket stability under various fin cant angles and crosswind speeds," Journal of Mechanical Engineering, vol. 22, no. 2, pp. 83-95, 2025, doi: 10.24191/jmeche.v22i2.2925.

[13] Z. Salleh, A. H. A. Hamid, A. A. Adnan, M. A. Muhammad, and S. Gwozdz, "The effects of fin cant angle and fin height on the performance of a low-altitude rocket," International Journal of Integrated Engineering, vol. 16, no. 8, pp. 300-310, 2024, doi: 10.30880/ijie.2024.16.08.030.

[14] R. A. Saylor, D. J. Royak, and J. P. Byron, "Rocket fin test fixture development and exploration of rotation-inducing fin design," University of Akron IdeaExchange, 2016.

[15] M. H. Shahir and A. Sapit, "A study on aerodynamic shape of fin of model rocket using computational fluid dynamics (CFD)," Research Progress in Mechanical and Manufacturing Engineering, vol. 2, no. 2, pp. 988-996, 2021, doi: 10.30880/rpmme.2021.02.02.107.

[16] H. Q. Yang, J. West, and R. E. Harris, "Coupled fluid-structure interaction analysis of solid rocket motor with flexible inhibitors," in Proc. 52nd Aerospace Sciences Meeting, 2014, pp. 1-24, doi: 10.2514/6.2014-1268.

[17] Z. Yang, C. Yang, J. Zhao, and Z. Wu, "Fluid-structure interaction dynamic response of rocket fairing in falling phase," Aerospace, vol. 9, no. 12, 2022, doi: 10.3390/aerospace9120741.